

# The two critical temperatures conundrum in $\text{La}_{1.875}\text{Sr}_{0.125}\text{CuO}_4$

Abhisek Samanta,<sup>1,\*</sup> Itay Mangel,<sup>2,†</sup> Amit Keren,<sup>2,‡</sup> Daniel P. Arovas,<sup>3,§</sup> and Assa Auerbach<sup>2,¶</sup>

<sup>1</sup>*Department of Physics, The Ohio State University, Columbus OH 43210, USA*

<sup>2</sup>*Physics Department, Technion, 32000 Haifa, Israel*

<sup>3</sup>*Department of Physics, University of California at San Diego, La Jolla, CA 92093, USA*

(Dated: September 1, 2023)

The in-plane and out-of-plane components of the stiffness tensor  $\rho_{\parallel}$  and  $\rho_{\perp}$  in  $\text{La}_{1.875}\text{Sr}_{0.125}\text{CuO}_4$ , show different transition temperatures, with strong variations of the latter on sample width. Disorder and critical finite size corrections are too small to explain these effects. With evidence from Monte Carlo simulations, we show that due to the high anisotropy, a three dimensional sample approaching the transition temperature  $T_c$  acts as a quasi one dimensional Josephson array. As such,  $\rho_{\perp}(T)$  exhibits an essential singularity  $\exp(-A/|T-T_c|^{2\beta})$ . At finite experimental or numerical resolution,  $\rho_{\perp}$  always appears to vanish at a lower temperature than the in-plane stiffness. An analogy to studies of helium superfluids in nanopores is made.

A homogeneous three-dimensional superconductor is expected to exhibit a single transition temperature  $T_c$  at which the order parameter,  $\Delta(T)$ , and all the superconducting stiffness components vanish [1, 2]. In this regard, recent experiments in LSCO crystals by Kapon *et. al.* [3] seem exceptional, in that they observe a substantial difference in the critical temperature in  $\text{La}_{1.875}\text{Sr}_{0.125}\text{CuO}_4$  as inferred from the behavior of the in-plane ( $\rho_{\parallel}$ ) and  $c$ -axis ( $\rho_{\perp}$ ) stiffnesses, with  $\rho_{\perp}(T)$  vanishing at a lower temperature, by about 0.64 K.

These results were obtained using a ‘stiffnessometer’ [4] comprised of a long excitation coil which pierces a superconducting ring. A bias current in the coil creates an Aharonov-Bohm vector potential  $A^{\gamma}$  which, by London’s equation, produces a persistent current that is measured by the induced magnetization  $m$ . Two rings, labelled *a* and *c*, were prepared with their coil axes parallel (*a*) and perpendicular (*c*) to the  $\text{CuO}_2$  planes. A measurement of  $m > 0$  indicates a nonzero stiffness component  $\rho_{\parallel}$  or  $\rho_{\perp}$  for the *c*- or *a*-ring, respectively.

In this paper we examine the effect of finite ring dimensions. We measure the *a*- and *c*-ring temperature-dependent magnetizations  $m(T)$  for varying widths. The rings were cut by a laser, or polished down to the geometries shown in Fig. 1(a-b). For the *a*-ring, we varied mostly the narrowest (bottleneck) widths of the *a* – *b* planes,  $L_a$ , whereas for the *c*-ring we varied both  $L_c$  and  $L_a$  (see Figs. 1(a,b)). Fig. 1(c) shows the narrowest bottleneck geometry of the *a*-ring. Fig. 1(d) shows a clear dependence of the *a*-ring magnetization vanishing temperatures on  $L_a$ . For comparison, the *c*-rings magnetization, depicted in Fig. 1(e), show curves extrapolating to a single transition temperature, (except for the  $L_a = 0.09$  mm sample, which might include a deep cut). More experimental details are given in the Supplementary Material (SM) [5].

The relative temperature shifts as a function of sample width are of order 1 – 10%, which are large and call

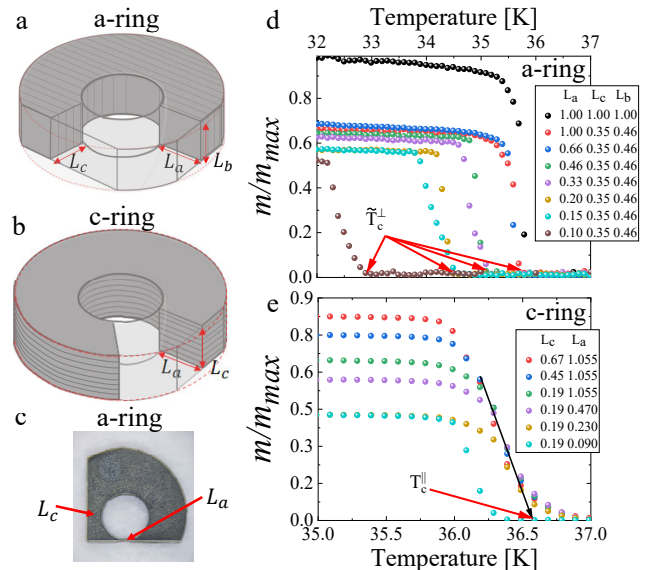


FIG. 1. Experimental configuration and magnetization data of  $\text{La}_{1.875}\text{Sr}_{0.125}\text{CuO}_4$ . (a) The interior of the *a*-ring with the  $\text{CuO}_2$  plane parallel to the ring’s symmetry axis. This ring is cut along two planes and polished thus modifying three bottleneck lengths:  $L_a$ ,  $L_b$ , and  $L_c$ . (b) The interior of the *c*-ring with the  $\text{CuO}_2$  plane perpendicular to the ring’s symmetry axis. This ring is cut along one plane and polished, thus controlling two bottleneck lengths  $L_a$  and  $L_c$ . (c) Photograph of an *a*-ring with two cut planes. (d) Magnetization data of *a*-rings with different dimensions. (e) Magnetization data of *c*-rings with different dimensions. The mean transition temperature  $T_{c,\parallel}$  is defined by a linear extrapolation of  $m(T)$  from below the correlated disorder-induced tail (see text). The narrowest sample  $L_a = 0.09$  mm, is suspected to contain a deep cut.  $m_{\max}$  stands for the  $T \rightarrow 0$  magnetization of the largest ring.

for theoretical explanation. Two obvious options were considered:

(i) Finite size effects due to critical fluctuations: Correlation lengths are much shorter than the millimeter scale

(see SM [5]) except unobservably near  $T_c$  [6, 7].

(ii) Disorder: Short range disorder is not expected to affect the critical behavior of a superconductor, by Harris's criterion [8]. On the other hand, correlated planar disorder [9, 10], or a small gradient in dopant concentration along the  $c$  axis, should broaden the transition in  $\rho_{\parallel}$ , and reduce the vanishing temperature of  $\rho_{\perp}$  [5]. Such inhomogeneities produce a high temperature tail above the mean critical temperature  $T_{c,\parallel}$ . The  $c$ -rings exhibit such a tail (see Fig. 1(e)) but its width is smaller than the differences of the  $a$ - and  $c$ -rings  $T_c$  values, and disorder is unlikely to account for the strong systematic width dependence of  $T_{c,\perp}$  as seen in Fig. 1(d).

The two  $T_c$ 's conundrum is resolved as an *apparent* shift in  $T_c$ 's, caused by an essential singularity of the  $c$  axis stiffness. To explain this effect, two fundamental characteristics of cuprate superconductors are taken into account:

(i)  $T_c$  is driven by phase fluctuations, as described by the classical  $XY$  model, rather than vanishing of the BCS gap [11]. This statement is supported by Uemura's empirical scaling of  $T_c \propto \rho_{\parallel}$  [12], combined with the jump in  $\rho_{\parallel}$  at  $T_c$  which is observed in ultra-thin films [13].

(ii) Cuprates are layered superconductors with extremely high anisotropy between inter-layer and intralayer stiffness coefficients. The superconducting order parameter  $\Delta(T)$  has a non-BCS, trapezoidal temperature dependence [14], which falls abruptly above the two dimensional Berezinskii-Kosterlitz-Thouless (BKT) [15] as shown in Fig. 2.

In the crossover regime of  $[T_{\text{BKT}}, T_c]$ , a three dimensional sample with nearly cubic aspect ratio, crosses over to behave as a quasi one dimensional Josephson junction array along the  $c$  axis. The  $c$ -axis stiffness near  $T_c$  goes as  $\rho_{\perp} \propto \exp(-K/\alpha L_a |T_c - T|^{2\beta})$ , where  $\alpha \ll 1$  is the anisotropy parameter,  $\beta$  is the order parameter's critical exponent.  $K$  is shown to be weakly (logarithmically) dependent on  $\alpha$  and on the experimental cut-off which determines the apparent transition temperature  $\tilde{T}_c^{\perp}$ .

The analytic formulas for  $\rho_{\perp}$  and  $K$  are confirmed by fitting them to the Monte Carlo data for the stiffness coefficient of the three dimensional anisotropic  $XY$  model. The same expressions are applied to describe the data, and fitted them with a new (reasonable) estimate of its anisotropy parameter to  $\alpha^{\text{fit}} = 3.4 \times 10^{-5}$ .

In the summary we discuss the analogy between the quasi one dimensional behavior of layered cuprates, and (isotropic) superfluid density of  ${}^4\text{He}$  embedded in quasi-one dimensional nanopores [16].

*Model*— We model the system by the three dimensional classical  $XY$  (3d $XY$ ) Hamiltonian on a tetragonal lattice,

$$H_{XY} = - \sum_i \sum_{\gamma} J_{\gamma} \cos(\varphi_{\mathbf{r}_i} - \varphi_{\mathbf{r}_i + \mathbf{a}_{\gamma}}) \quad . \quad (1)$$

where  $\gamma \in \{a, b, c\}$  and where  $J_{a,b} = J_{\parallel}$  and  $J_c = J_{\perp}$  are

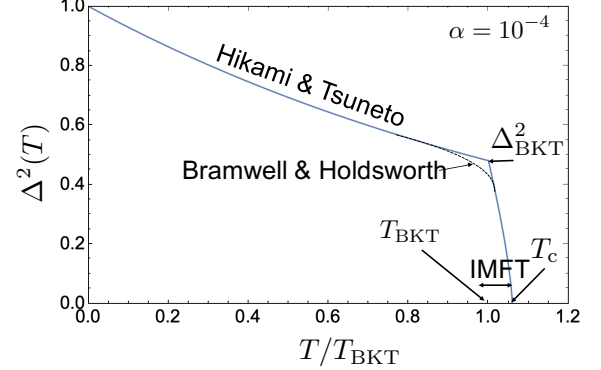


FIG. 2. The order parameter squared as a function of temperature for the layered classical  $XY$  model. The graph patches the linear spinwave theory of Hikami and Tsuneto [22], the crossover (dashed line) power law of Bramwell and Holdsworth [19], and the three dimensional critical point which is obtained by Interplane Mean Field Theory (IMFT) of Eqs. (2), (3) and (4).

the effective intra- and inter-plane Josephson couplings. The anisotropy parameter  $\alpha = J_{\perp}/J_{\parallel}$  will be fit to the experiments. Our temperature units are taken as  $k_{\text{B}} = 1$ . The effective lattice constants for the  $XY$  model's lattice are taken to be the Cooper-pair dimensions, as defined by the zero temperature coherence lengths  $\xi_{\parallel,0}$  and  $\xi_{\perp,0}$ .

Decoupled layers ( $\alpha = 0$ ) have a vanishing order parameter  $\Delta = \langle e^{i\varphi} \rangle = 0$  but a finite in-plane stiffness up to the Berezinskii-Kosterlitz-Thouless [15] transition at  $T_{\text{BKT}} \simeq 0.893 J_{\parallel}$ . Interlayer mean field theory (IMFT) is applicable for high anisotropy  $0 < \alpha \ll 1$  [14, 17–20]. It predicts a finite order parameter below the three dimensional critical temperature  $T_c$  which is slightly higher than  $T_{\text{BKT}}$ ,

$$\frac{T_c - T_{\text{BKT}}}{T_{\text{BKT}}} = \left( \frac{b}{|\ln(0.14\alpha)|} \right)^2 \quad . \quad (2)$$

Here, the (non universal) constant is taken to be  $b = 2.725$  [21].

In the regime  $[0, T_{\text{BKT}}]$ , the order parameter magnitude  $\Delta = |\langle e^{i\varphi} \rangle|$  decreases from unity as calculated by Hikami and Tsuneto [22],

$$\Delta^2(T)_{T \leq T_{\text{BKT}}} \simeq \exp \left( - \frac{T \log(1/\alpha)}{4\pi J_{\parallel}} \right) \quad . \quad (3)$$

Over the crossover regime  $T \in [T_{\text{BKT}}, T_c]$ , the order parameter initially crosses over with an intermediate power law of  $|T - T^*|^{0.23}$  [19], and then drops precipitously to zero toward the 3d $XY$  model transition temperature  $T_c$ , with

$$\Delta^2(T) = m_{\text{BKT}}^2 t^{2\beta} \quad , \quad t \equiv \left( \frac{T_c - T}{T_c - T_{\text{BKT}}} \right) \quad , \quad (4)$$

where  $\beta$  crosses over to  $\beta = 0.349$  very close to  $T_c$  [14]. As shown in Fig. (2), the order parameter exhibits a smoothed ‘trapezoidal’ temperature dependence, which differs from the typical temperature dependence of the BCS gap in conventional (weak coupling) superconductors [14].

The superfluid stiffness component of the 3dXY model near criticality are

$$\rho_\gamma(T) = \rho_\gamma(T_{\text{BKT}}) t^s, \quad (5)$$

where  $s$  is the stiffness critical exponent given by [1]

$$s = 2\beta - \eta\nu \simeq 2\beta. \quad (6)$$

$\eta$  and  $\nu$  are the critical correlation function power law and correlation length exponents respectively. For our system,  $\eta\nu = 0.0255$  is numerically negligible.

The *apparent* premature vanishing of  $\rho_\perp$  in a finite sample of an approximately unit aspect ratio, is due to its crossover to a quasi one-dimensional behavior as  $T \rightarrow T_c$ . The stiffness of a purely one dimensional (1d) classical XY model with Josephson coupling  $J_{1d}$ , lattice constant  $a$  and overall length  $L$  is given exactly by

$$\begin{aligned} \rho_{1d}(T, L) &= TLZ_2/Z_0 \\ Z_{2p} &= \sum_{n=-\infty}^{\infty} \left( \frac{I_n(J_{1d}/T)}{I_0(J_{1d}/T)} \right)^{L/a} n^{2p} \end{aligned} \quad (7)$$

where  $I_n$  are modified Bessel functions and  $p = 0, 1$ . By Luttinger liquid (LL) theory [23, 24], for large  $L \gg a$ ,  $\rho_{1d}$  depends on the scale variable  $x \equiv LT/J_{1d}a$  as

$$\begin{aligned} \rho_{\text{LL}}(J_{1d}, x) &= J_{1d}a \left( 1 - \frac{\pi^2}{x} \frac{\vartheta_3''(0, e^{-2\pi^2/x})}{\vartheta_3(0, e^{-2\pi^2/x})} \right) \\ &\simeq J_{1d}a \begin{cases} 1 & (x \leq 2) \\ 20 \exp(-0.472x) & (x \geq 10) \end{cases}. \end{aligned} \quad (8)$$

where  $\vartheta_3(z, q) = 1 + 2 \sum_{n=1}^{\infty} q^{n^2} \cos(2nz)$ , and prime denotes differentiation with respect to  $z$ . Comparison between eqs. (7) and (8) is shown in the SM [5].

Strictly speaking  $\rho_\perp(T, L_a)$  does not vanish at  $T < T_c$ . However, as  $\Delta^2(T) \rightarrow 0$  decreases toward  $T_c$ , the layered superconductor crosses over to behave as an effectively quasi-1d array with an effective inter-plane coupling given by

$$J_{\text{eff}}(T) = \frac{L_a L_b}{\xi_{\parallel,0}^2} \times J_\perp \Delta^2(T), \quad (9)$$

where  $\Delta^2$  vanishes as  $t^{2\beta}$  by Eq. (4). The geometric aspect ratio of the ring is defined as  $r = L_c/L_b$  which is of order unity.

Inserting  $x(T) = L_c/\xi_{\perp,0} J_{\text{eff}}(T)$  and using Eqs. (8) and (9), the normalized  $c$ -axis stiffness vanishes as

$$\rho_\perp(T) \approx 20 \rho_\perp(0) \exp(-C t^{-2\beta}), \quad (10)$$

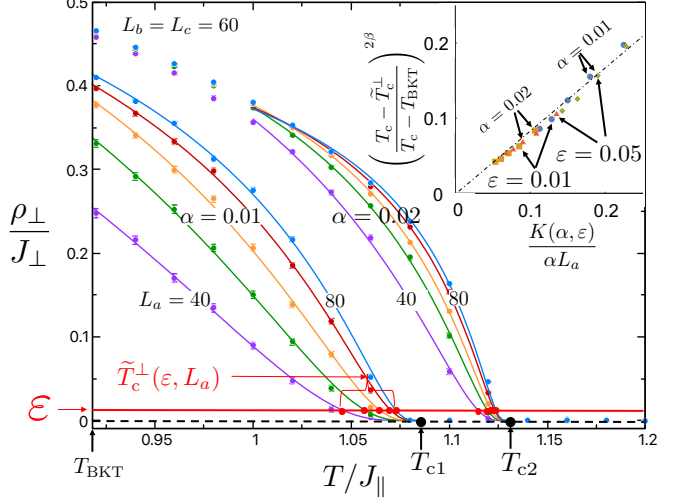


FIG. 3. MC evaluations of  $\rho_\perp$  as a function of temperature for a range of sample widths  $L_a \in \{40, 50, \dots, 80\}$ , and anisotropy parameters  $\alpha$ . The thermodynamic critical temperatures are evaluated as  $T_{c1} = 1.086J_\parallel$  and  $T_{c2} = 1.13J_\parallel$  for  $\alpha = 0.01$  and  $0.02$ , respectively. Solid lines are best fits to Eq. (10). The  $\varepsilon$  values are arbitrarily chosen resolutions which define the apparent transition temperatures  $\tilde{T}_{c,\perp}^\perp$ . Inset: Collapse of the temperature shifts obtained from the main graphs, using the three dimensional critical exponent  $\beta = 0.349$  and the coefficients  $K(\alpha, \varepsilon)$  as defined in Eq. (13).

where

$$C \simeq \frac{0.472 r T_c \xi_{\parallel,0}^2}{J_\parallel \Delta_{\text{BKT}}^2 \xi_{\perp,0}} \times \frac{1}{\alpha L_a}. \quad (11)$$

For any experimental resolution  $\varepsilon$ , an apparent vanishing temperature  $\tilde{T}_{c,\perp}(\varepsilon)$  can be defined by equating

$$\rho_\perp(\tilde{T}_{c,\perp}) \equiv \varepsilon \rho_\perp(0). \quad (12)$$

Using Eq. (10), the apparent width dependent transition temperature is,

$$\begin{aligned} T_c - \tilde{T}_{c,\perp} &= (T_c - T_{\text{BKT}}) \left( \frac{K(\alpha, \varepsilon, r)}{\alpha L_a} \right)^{1/2\beta} \\ K &\equiv \frac{0.472 r T_c \xi_{\parallel,0}^2}{J_\parallel \Delta_{\text{BKT}}^2 \xi_{\perp,0} \log(20/\varepsilon)} \end{aligned} \quad (13)$$

where the coefficient  $K$  is proportional to  $r$  and weakly (logarithmically) dependent on  $\alpha$  and  $\varepsilon$ . The most important consequence of the quasi one-dimensional behavior, is that the temperature shifts are proportional to  $(\alpha L_a)^{-1/2\beta}$ , which is a much larger effect than from finite size scaling, which goes as  $(\alpha L_a^2)^{-1}$  [5].

*Monte Carlo simulations* – The superfluid stiffness (*i.e.* helicity modulus) of  $H_{XY}$ , with  $a_\gamma = 1$ , is given by [16],

25]

$$\rho_\gamma = \frac{J_\gamma}{V} \left\langle \sum_{\langle ij \rangle} \cos(\varphi_{\mathbf{r}_i} - \varphi_{\mathbf{r}_j}) (r_i^\gamma - r_j^\gamma)^2 \right\rangle \quad (14)$$

$$- \frac{J_\gamma^2}{VT} \left\langle \left( \sum_{\langle ij \rangle} \sin(\varphi_{\mathbf{r}_i} - \varphi_{\mathbf{r}_j}) (r_i^\gamma - r_j^\gamma) \right)^2 \right\rangle ,$$

with  $V = L_a L_b L_c$ . The first contribution measures the short range correlations, which are proportional to minus the energy along the bonds in the  $\gamma$  direction. The second contribution measures long range current fluctuations, which vanish at zero temperature, and reduce the stiffness at finite temperatures.

To verify Eq. (13) we apply a Monte Carlo (MC) simulation of  $H_{XY}$  with the Wolff cluster updates algorithm [26]. We choose  $L_c = L_b = 60$ , and vary the width in the range  $L_a \in \{40, 50, \dots, 80\}$  using the anisotropy parameters  $\alpha = 0.01$  and  $0.02$ .

In Fig. 3, the MC results for  $\rho_\perp(T)$  are shown. They exhibit similar effects as seen experimentally at much larger systems, and smaller values of  $\alpha$ . Within numerical resolution  $\varepsilon$ ,  $\rho_\perp(T)$  drops down below and appears to vanish, within the numerical uncertainty of magnitude  $\varepsilon$ . We use least square fits to determine  $\tilde{T}_c(L_a, \alpha)$ , and the values of  $K(\alpha, \varepsilon)$  from Eq. (10). The relative temperature shifts data collapse onto a straight line verifying the detailed functional form of  $\rho_\perp(T)$ . The slope of this line differs only by 20% from unity which is defined by the asymptotic forms of Eq. (8).

In the SM [5] we show that  $\rho_\parallel(T)$ , in contrast to  $\rho_\perp$ , survives slightly *above*  $T_c$ . This is a consequence of the relatively small planes' dimensions in the MC simulation, and the long in-plane phase correlations which survive above  $T_c$  even in the limit  $\alpha \rightarrow 0$ . These effects are too small in the experimental samples' dimensions.

*Comparison of theory to experiment* – An experimental relative resolution of  $\varepsilon = 10^{-2}$  determines the apparent transition temperature  $\tilde{T}_c^\perp(L_a, \varepsilon)$  as the lowest temperature which obeys  $m(\tilde{T}_c^\perp, L_a) = \varepsilon m_{\max}$ , where  $m_{\max}$  is the zero temperature magnetization of the largest ring.

In Fig. 4, the transition temperature shifts in the  $a$ -rings are plotted versus  $L_a$ . The data is somewhat noisy, presumably because of introduction of deep cuts during the ring's cutting process, which are eliminated by subsequent cuts.

To explain the experimental data we set the parameters of  $H_{XY}$  as follows. The lattice constants are taken as the zero temperature coherence lengths [14] estimated experimentally to be [27]

$$\xi_{\parallel,0} \simeq 3 \text{ nm} \quad , \quad \xi_{\perp,0} \simeq 1.3 \text{ nm} \quad . \quad (15)$$

The couplings are related to the London penetration

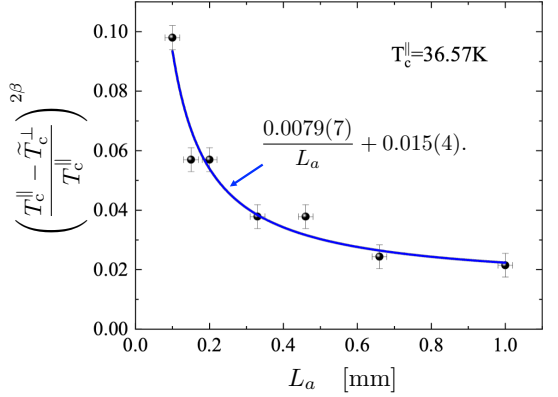


FIG. 4. Comparison of experiment and theory. Crosses: The apparent transition temperature shifts given by  $\tilde{T}_c^\perp$  and  $T_{c,\parallel}$  as defined in fig. 1(d) and (e).  $L_a$  are the bottleneck widths of the  $ab$  planes in the  $a$  rings. Line: the least square fit which is used to determine  $\alpha^{\text{fit}} = 3.4 \times 10^{-5}$ , and the offset of the apparent transition temperature at infinite width, Eq. (18). Due to the narrow Ginzburg fluctuations regime, the mean field exponent  $\beta = \frac{1}{2}$  is used for the fit.

depths by the relations [14],

$$J_\parallel = \frac{\xi_{\perp,0} \hbar^2 c^2}{\lambda_a^2 16\pi e^2} \quad , \quad J_\perp = \frac{\xi_{\parallel,0}^2 \hbar^2 c^2}{\xi_{\perp,0} \lambda_c^2 16\pi e^2} \quad . \quad (16)$$

$e$  and  $c$  are the electron charge and the speed of light, respectively. It should be pointed out that  $\lambda_c$  in  $\text{La}_{1.875}\text{Sr}_{0.125}\text{CuO}_4$  was measured in Ref. [28] in magnetically oriented powder to be as large as  $8.5 \mu\text{m}$ . In a low energy muon experiment on a single crystal [3],  $\lambda_c$  appeared to be too long to be detectable. Therefore, our stiffnessometer measurements can provide a more direct determination of  $\alpha$  in a single crystal. Taking  $\lambda_a = 0.27 \mu\text{m}$  [29], and  $\xi_\gamma$  from Eq. (15), yields the estimate of  $\lambda_c = 21 \mu\text{m}$  for our samples.

We find that the data of Fig. 4 can be fit by our Eq.(13) taking  $\alpha^{\text{fit}} = 3.4 \times 10^{-5}$ . By Eqs. (13) and (3),

$$\frac{T_c(\alpha) - T_{\text{BKT}}}{T_c} = 0.049 \quad , \quad m_{\text{BKT}}^2 = 0.44 \quad . \quad (17)$$

The  $a$ -ring is cut such that the induced current is confined effectively in a section of dimensions  $L_b = 0.46 \text{ mm}$ ,  $L_c = 2 \text{ mm}$ , which yields  $r = 4.34$ . The width varies in the range  $L_a \in [0.1, 1] \text{ mm}$ .

The minimal relative experimental resolution is  $\varepsilon = 10^{-2}$ . For the fitted  $\alpha^{\text{fit}} = 3.4 \times 10^{-5}$  we obtain  $K = 0.257 \text{ nm}$ , which reproduces the coefficient of 0.0079 of the least squares fit in Fig. (1), with an offset of 0.015 for the transition temperatures of  $\rho_\perp$  at large width

$$\lim_{L_a \rightarrow \infty} \tilde{T}_{c,\perp} \approx 0.985 T_{c,\parallel} \quad . \quad (18)$$

This correction can be attributed to correlated disorder [9, 10], or a weak gradient of doping concentrations

along the  $c$  axis, as explained in the SM [5]. While  $T_{c,\parallel}$  is determined by the arithmetic mean of  $\rho_{\parallel}(z)$  for  $z \in [0, L_c]$ ,  $\rho_{\perp}$  is proportional to the *harmonic* mean, which is dominated by sections with minimal order parameter. Therefore  $\rho_{\perp}$  vanishes at a lower temperature than  $T_{c,\parallel}$ , even for  $L_a \rightarrow \infty$ .

*Analog in  $^4\text{He}$*  – We have seen that  $\alpha \ll 1$  can be mapped onto an isotropic model on samples with large aspect ratio. A similar “premature” vanishing of  $\rho_{\perp}$  has been observed on a quasi-one dimensional brick, *i.e.*  $L_a \ll L_c$  [16]. This result was used to explain the experimental disappearance of superfluid density of  $^4\text{He}$  embedded in quasi one-dimensional nanopores [30, 31]. Here we explain the *apparent* reduction of  $\tilde{T}_c(L_a)$ , not as a true thermodynamic transition but rather as a consequence of an essential singularity decay of  $\rho_{\perp}$  toward the thermodynamic  $T_c$ .

*Acknowledgements* – We thank Erez Berg, Snir Gazit, Michel Gingras, Dror Orgad, Daniel Podolsky and Thomas Vojta for beneficial discussions. AA acknowledge the Israel Science Foundation (ISF) Grant No. 2081/20. AK acknowledges the ISF Grant. No. 1251/19 and 3875/21. This work was performed in part at the Aspen Center for Physics, which is supported by National Science Foundation grant PHY-2210452, and at the Kavli Institute for Theoretical Physics, supported by Grant No. NSF PHY-1748958.

Statt, C. E. Stronach, W. J. Kossler, and X. H. Yu, *Phys. Rev. Lett.* **62**, 2317 (1989).

[13] I. Hetel, T. R. Lemberger, and M. Randeria, *Nat. Phys.* **3**, 700 (2007).

[14] A. Mihlin and A. Auerbach, *Phys. Rev. B* **80**, 134521 (2009).

[15] J. M. Kosterlitz and D. J. Thouless, *Jour. Phys. C: Sol. State Phys.* **6**, 1181 (1973).

[16] A. Kotani, K. Yamashita, and D. S. Hirashima, *Phys. Rev. B* **83**, 174515 (2011).

[17] D. J. Scalapino, Y. Imry, and P. Pincus, *Phys. Rev. B* **11**, 2042 (1975).

[18] B. Keimer, A. Aharony, A. Auerbach, R. J. Birgeneau, A. Cassanho, Y. Endoh, R. W. Erwin, M. A. Kastner, and G. Shirane, *Phys. Rev. B* **45**, 7430 (1992).

[19] S. T. Bramwell and P. C. W. Holdsworth, *Phys. Rev. B* **49**, 8811 (1994).

[20] P. Butera and M. Pernici, *Phys. Rev. B* **80**, 054408 (2009).

[21] J. M. Kosterlitz, *Jour. Phys. C: Sol. State Phys.* **7**, 1046 (1974).

[22] S. Hikami and T. Tsuneto, *Prog. Theor. Phys.* **63**, 387 (1980).

[23] A. Del Maestro and I. Affleck, *Phys. Rev. B* **82**, 060515 (2010).

[24] D. S. Hirashima, *Phys. Rev. B* **102**, 104506 (2020).

[25] S. Teitel and C. Jayaprakash, *Phys. Rev. B* **27**, 598 (1983).

[26] U. Wolff, *Phys. Rev. Lett.* **62**, 361 (1989).

[27] I. Mangel and A. Keren, arXiv:2308.06757.

[28] C. Panagopoulos, J. R. Cooper, T. Xiang, Y. S. Wang, and C. W. Chu, *Phys. Rev. B* **61**, R3808 (2000).

[29] C. Panagopoulos, B. D. Rainford, J. R. Cooper, W. Lo, J. L. Tallon, J. W. Loram, J. Betouras, Y. S. Wang, and C. W. Chu, *Phys. Rev. B* **60**, 14617 (1999).

[30] N. Wada, J. Taniguchi, H. Ikegami, S. Inagaki, and Y. Fukushima, *Phys. Rev. Lett.* **86**, 4322 (2001).

[31] R. Toda, M. Hieda, T. Matsushita, N. Wada, J. Taniguchi, H. Ikegami, S. Inagaki, and Y. Fukushima, *Phys. Rev. Lett.* **99**, 255301 (2007).

[32] F. Hrahsheh and T. Vojta, *Phys. Scripta* **2012**, 014074 (2012).

[33] A. W. Sandvik, in *AIP Conference Proceedings*, Vol. 1297 (American Institute of Physics, 2010) pp. 135–338.

\* samanta.12@osu.edu

† itaymangelsavir@gmail.com

‡ phkeren@technion.ac.il

§ darovas@ucsd.edu

¶ assa@physics.technion.ac.il

[1] M. E. Fisher, M. N. Barber, and D. Jasnow, *Phys. Rev. A* **8**, 1111 (1973).

[2] M. Hasenbusch, *Phys. Rev. B* **100**, 224517 (2019).

[3] I. Kapon, Z. Salman, I. Mangel, T. Prokscha, N. Gavish, and A. Keren, *Nat. Comm.* **10**, 2463 (2019).

[4] I. Mangel, I. Kapon, N. Blau, K. Golubkov, N. Gavish, and A. Keren, *Phys. Rev. B* **102**, 024502 (2020).

[5] “Supplementary Material.”.

[6] Y.-H. Li and S. Teitel, *Phys. Rev. B* **40**, 9122 (1989).

[7] J. Cardy, *Finite-size scaling (Chapter 1)* (Elsevier, 2012).

[8] A. B. Harris, *Jour. Phys. C: Sol. State Phys.* **7**, 1671 (1974).

[9] P. Mohan, P. M. Goldbart, R. Narayanan, J. Toner, and T. Vojta, *Phys. Rev. Lett.* **105**, 085301 (2010).

[10] D. Pekker, G. Refael, and E. Demler, *Phys. Rev. Lett.* **105**, 085302 (2010).

[11] V. J. Emery and S. A. Kivelson, *Nature* **374**, 434 (1995).

[12] Y. J. Uemura, G. M. Luke, B. J. Sternlieb, J. H. Brewer, J. F. Carolan, W. N. Hardy, R. Kadono, J. R. Kempton, R. F. Kiefl, S. R. Kreitzman, P. Mulhern, T. M. Riseman, D. L. Williams, B. X. Yang, S. Uchida, H. Takagi, J. Gopalakrishnan, A. W. Sleight, M. A. Subramanian, C. L. Chien, M. Z. Cieplak, G. Xiao, V. Y. Lee, B. W.

## The two critical temperatures conundrum in $\text{La}_{1.875}\text{Sr}_{0.125}\text{CuO}_4$

### Supplementary Material

For the anisotropic three dimensional  $XY$  model, we show that the finite size effects on the transition temperature are unobservably small, but planar correlated disorder produces a lower transition temperatures for  $\rho_{\perp}$  than for  $\rho_{\parallel}$ . The stiffness of the finite one dimensional  $XY$  chain is shown to asymptotically agree with the Luttinger liquid formula, used in the main text. We provide additional experimental details of the stiffness measurements, and numerical details of the Monte Carlo simulations.

#### ESTIMATION OF FINITE SIZE SHIFT IN $T_c$

Fine size scaling produce unobservably small finite size shifts of  $T_c$  as shown by the following. The correlation lengths above  $T_{\text{BKT}}$  diverge as

$$\xi_{\parallel}(t) \simeq \frac{1}{\sqrt{\alpha}} \xi_a^{(0)} t^{-\nu}, \quad \xi_{\perp}(t) \simeq \xi_c^{(0)} t^{-\nu} \quad (19)$$

where we use the Ginzburg Landau definition of correlation lengths,  $\xi_{\gamma}^{-1} \propto \sqrt{\rho_{\gamma}}$ , to obtain the factor of  $\sqrt{\alpha}$  between the divergent correlation length.

For Eq. (27) with sample dimensions  $L_{\gamma}, \gamma = a, b, c$  the stiffness components near  $T_c$  vanish as [6],

$$\frac{\rho_{\perp}}{\rho_{\perp}(T_{\text{BKT}})} = t^{\nu} \Phi[x_a], \quad x_a = \xi_a(t)/L_a. \quad (20)$$

where  $\Phi(x)$  is differentiable function with a finite value at  $x = 0$ . We expand  $\Phi$  to linear order in  $x_i a$  and set  $\rho_{\perp} \rightarrow 0$  to obtain,

$$0 = \Phi_0 + \partial_{x_a} \Phi \times \left( \frac{t^{-\nu} \xi_a^{(0)}}{\sqrt{\alpha} L_a} \right) + \mathcal{O}(x_a^2) \quad (21)$$

which is solved by a positive shift of  $T_c$  by the amount

$$\delta t \simeq -\frac{\Phi_0}{\partial_a \Phi_{\gamma}} \left( \frac{\sqrt{\alpha} L_a}{\xi_a^{(0)}} \right)^{-\frac{1}{\nu}} \quad (22)$$

For the experimental  $\text{La}_{1.875}\text{Sr}_{0.125}\text{CuO}_4$  rings,  $L_a/\xi_a^{(0)} \sim 10^6$ , which yields  $|\delta t| \leq 10^{-4}$ , which is much below experimental temperature resolution.

#### PLANAR CORRELATED DISORDER

Refs. [9, 10] have considered the layered  $XY$  model where the  $ab$  planes exhibit a variable  $z$ -dependent stiffness  $\rho_{\parallel}(z)$  for  $z \in [0, L_c]$ . We can see the effects of this correlated disorder on systems with slow variation of  $\rho_{\parallel}(z)$ . In each segment, the critical behavior of the stiffness is

$$\rho_{\parallel}(T) = \rho_{\parallel}(0) |T - T_c^{\parallel}(z)|^{2\beta - \eta\nu} \quad (23)$$

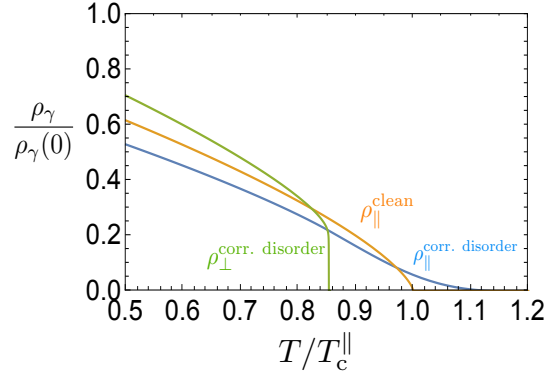


FIG. 5. Depiction of the effect of planar-correlated disordered  $\rho_{\parallel}(z)$ , with an average transition temperature  $T_c^{\parallel}$  and a width of transition temperatures  $\delta T_c = 0.1 T_c^{\parallel}$ . Orange line: The clean system with a three dimensional critical behavior. Blue line: the global  $\rho_{\parallel}^{\text{cor. disorder}}$  showing a disorder induced high temperature tail above  $T_c^{\parallel}$ . Green line: the global  $\rho_{\perp}^{\text{cor. disorder}}$ , which is dominated by the weakest interplane stiffnesses, and vanishes below  $T_c^{\parallel}$ .

where  $T_c^{\parallel}(z) \propto \rho_{\parallel}(z, 0)$  is the local transition temperature whose average is defined as  $T_c^{\parallel}$  and its variance is  $\delta T_c$ . The global  $ab$ -stiffness is given by the integral

$$\rho_{\parallel} = \rho_{\parallel}(0) \frac{1}{L_c} \int_0^{L_c} dz |T - T_c(z)|^{2\beta - \eta\nu} \quad (24)$$

which smears the average critical temperature  $T_c^{\parallel}$  by a high temperature tail of width  $\delta T_c$ .

In contrast, the  $c$ -axis stiffness  $\rho_{\perp}(z)/\rho_{\perp}(0)$  is proportional to the local order parameter squared  $\Delta(z)^2 = |T - T_c(z)|^{2\beta}$ . The global  $c$ -axis stiffness is the harmonic average given by,

$$\rho_{\perp} = \frac{\rho_{\perp}(0)}{L_c} \left( \int_0^{L_c} dz \frac{1}{L_a^2 |T - T_c(z)|^{2\beta}} \right)^{-1} \quad (25)$$

The weakest segments (minimal  $\rho_{\perp}(z)$ ), dominate the integral. In particular, at temperatures where some of the segments have vanishing  $\Delta(T, z) = 0$ , the whole integral vanishes. Therefore in effect,  $\rho_{\perp}(T)$  identically vanishes at a lower temperature than  $T_c^{\parallel}$ . This is demonstrated

in Fig. 5, for a gaussian distribution of the  $T_c$ 's of  $\rho_{\parallel}(z)$  and  $\Delta^2(z)$ , of width  $\delta T_c = 0.1 T_c^{\parallel}$ .

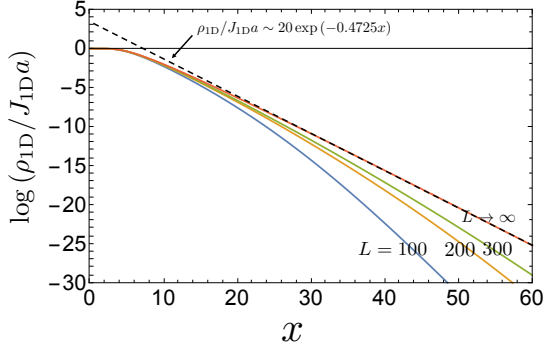


FIG. 6. Stiffness as a function of scaled variable  $x = LT/(J_{1D}a)$  in the one dimensional XY model for different lengths  $L$  as given by the exact result of Eq. (7), and asymptotically at  $L \rightarrow \infty$  by Eq. (8) of the main text.

#### ASYMPTOTIC BEHAVIOR OF STIFFNESS OF A ONE DIMENSIONAL XY CHAIN

In Fig. 6 we depict the exact result of the stiffness of the one dimensional XY chain as given by Eq. (7) of the main text. At large  $L/a$  the graphs show convergence to the analytic Luttinger-Liquid form [23, 24], which at large  $x$  is given by Eq. (8) of the main text.

#### EXPERIMENT

The experiment is base on a long excitation coil (EC) piercing a superconducting ring. At  $T \rightarrow T_c$ , the approximate London equation  $j_{sc} = -\rho A_{ec}$ , where  $j_{sc}$  is the current density in the coil and  $A_{ec}$  is the vector potential of the coil, ensures a finite current density in the ring. One then measures the magnetic moment of the ring  $m$  by moving a pickup loop relative to the ring and coil. The apparatus is shown in Fig. 7. For a perfect ring

$$m = h \int_{r_{in}}^{r_{out}} dr \pi r^2 j_{sc}(r) = -\frac{1}{4} \rho \Phi h (r_{out}^2 - r_{in}^2) , \quad (26)$$

where  $h$ ,  $r_{in}$ , and  $r_{out}$  are the ring's height, and inner and outer radii, and  $\Phi$  is the flux produced by the coil. From these measurements, the stiffness can be extracted. For irregular rings the situation is more complicated, but the critical temperature of the stiffness is still measurable.

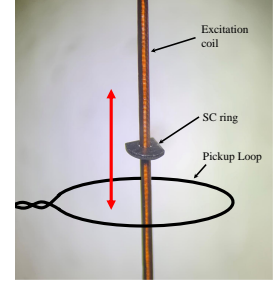


FIG. 7. A superconducting ring cut in two directions, on the excitation coil. The red double arrow shows the moving direction of the schematic pickup-loop relative to both coil and ring.

#### DETAILS OF THE MONTE-CARLO SIMULATIONS USING CLUSTER ALGORITHM

The Hamiltonian for the classical XY model on a tetragonal lattice is given by

$$H_{XY} = - \sum_{i,\gamma} J_{\gamma} \cos(\varphi_{\mathbf{r}_i} - \varphi_{\mathbf{r}_i + \mathbf{a}_{\gamma}}) , \quad (27)$$

where  $J_{a,b} = J_{\parallel}$ , and  $J_c = J_{\perp}$  are the effective intra-plane and inter-plane Josephson couplings respectively.  $\alpha = J_{\perp}/J_{\parallel}$  is the ratio of inter-plane and intra-plane couplings or the anisotropy parameter used in the main text. The superfluid stiffness or the helicity modulus (with  $a_{\gamma} = 1$ ) is given by [16, 25, 32]

$$\rho_{\gamma}(T) = \frac{J_{\gamma}}{V} \left\langle \sum_{\langle ij \rangle} \cos(\varphi_{\mathbf{r}_i} - \varphi_{\mathbf{r}_j}) (r_i^{\gamma} - r_j^{\gamma})^2 \right\rangle \quad (28)$$

$$- \frac{J_{\gamma}^2}{VT} \left\langle \left( \sum_{\langle ij \rangle} \sin(\varphi_{\mathbf{r}_i} - \varphi_{\mathbf{r}_j}) (r_i^{\gamma} - r_j^{\gamma}) \right)^2 \right\rangle ,$$

where  $V = L_a L_b L_c$  and  $\langle ij \rangle$  corresponds to a bond involving sites  $i$  and  $j$ .

In the Wolff-cluster algorithm, we assume the XY spins  $\mathbf{S}$  to be the unit vectors in  $\mathbb{R}^3$ . In every monte-carlo (MC) step, we first choose a random site  $\mathbf{r} \in \mathbb{R}_3$  and a random direction  $\mathbf{d} \in S_2$ , and consider a reflection of the spin on that site about the hyperplane orthogonal to  $\mathbf{d}$ . Note that this is equivalent to the spin-flipping operation in Ising model. We then travel to all neighboring sites  $(\mathbf{r}')$  of  $\mathbf{r}$ , and check if the bond  $\langle \mathbf{r} \mathbf{r}' \rangle$  is activated with a probability

$$P_{\gamma}(\mathbf{r}, \mathbf{r}') = 1 - \exp(\min[0, 2J_{\gamma}\beta(\mathbf{d} \cdot \mathbf{S}_{\mathbf{r}})(\mathbf{d} \cdot \mathbf{S}_{\mathbf{r}'})]) , \quad (29)$$

where  $\beta$  is the inverse temperature. If this satisfies, we mark  $\mathbf{r}'$  and include it to a cluster  $\mathcal{C}$  of “flipped” spins. We iteratively continue this process for all unmarked neighboring sites of  $\mathbf{r}'$  and grow the cluster size until

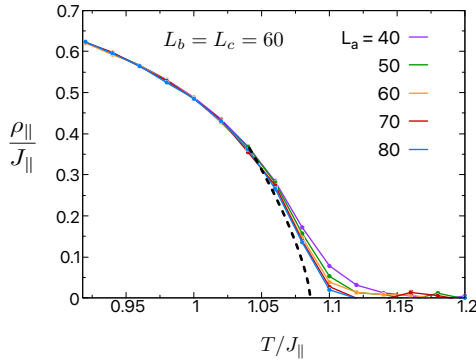


FIG. 8. The intra-plane helicity modulus or stiffness  $\rho_{\parallel}$ , plotted as a function of temperature  $T$ , for  $\alpha = 0.01$  and for different  $L_a$  between 40 and 80, while  $L_b$  and  $L_c$  are kept fixed at 60. The error bars are also shown at every  $T$ , which are smaller than the point sizes. The black dashed line shows the expected thermodynamic behavior near the transition.

all the neighbors turn out to be marked. We use such  $10^6$  number of MC steps for thermalization, followed by another  $10^7$  number of MC steps for measurement of different observables, such as the helicity modulus and the binder cumulant. We estimate the errors of different observables by using a standard Jackknife analysis of the MC data.

In Fig. 3 of the Main text, we have presented the inter-plane superfluid stiffness  $\rho_{\perp}$  for different system sizes of  $L_a \in [60 - 80]$ ,  $L_b = L_c = 60$ , near the transition. Here, in Fig. 8, we plot the intra-plane stiffness  $\rho_{\parallel}$  as a function of temperature  $T$ , for the same system sizes and for an anisotropic parameter  $\alpha = 0.01$ . We note that unlike  $\rho_{\perp}$ ,  $\rho_{\parallel}$  falls to zero much more slowly. However, we observe that increasing system size (i.e. increasing  $L_a$  in Fig. 8) makes the vanishing of  $\rho_{\parallel}$  sharper. We expect that in the thermodynamic limit  $\rho_{\parallel}$  will also vanish exactly at  $T_c$ , shown in the  $\rho_{\perp}$  graphs of the Main text. We therefore use a fitting function  $f(T) = a(T_c - T)^{2\beta}$  between the temperature where the  $\rho_{\parallel}$  curves for different

sizes start to deviate and the transition temperature  $T_c$  (which is  $\sim 1.086$  for these parameters) to show the expected thermodynamic behavior – this is shown by a dashed line in Fig. 8.

Next we calculate the binder cumulant, defined in terms of the higher powers of magnetization  $m$  as following [33]

$$U_2 = \frac{3}{2} \left( 1 - \frac{1}{3} \frac{\langle m^4 \rangle}{\langle m^2 \rangle^2} \right), \quad (30)$$

and we use it to extract the value of critical temperatures accurately. As an example, in Fig. 9, we present  $U_2$  as a function of  $T$ , for an anisotropy parameter  $\alpha = 0.005$  and for different system sizes with a fixed aspect ratio  $L_a = L_b$  and  $L_a/L_c = 16$ . In the ordered phase when all the spins are aligned it takes a value 1, while in the

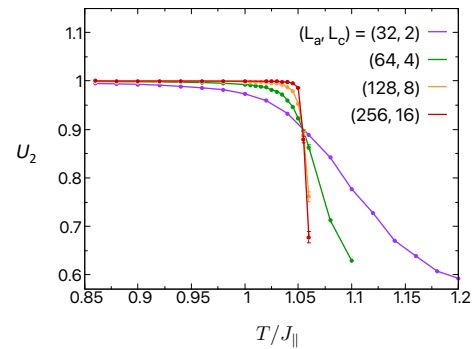


FIG. 9. Binder cumulant  $U_2$  plotted as a function of temperature  $T$ , for anisotropy  $\alpha = 0.005$  and for different sizes with a fixed aspect ratio  $L_a/L_c = 16$  and  $L_b = L_a$ .

disordered phase it vanishes and takes an intermediate value between 0 and 1 at the critical point. Therefore, by tracking the crossing between different system sizes, we find a critical temperature  $T_c \sim 1.05$  for these parameters. Using a similar analysis, we obtain  $T_c$  for other anisotropy parameters also, discussed in the Main text.